Journal of Atmospheric and Solar-Terrestrial Physics 177 (2018) 84–91

Contents lists available at ScienceDirect

Journal of Atmospheric and Solar-Terrestrial Physics

journal homepage: www.elsevier.com/locate/jastp

Magnetospheric Multiscale Observations of Turbulent Magnetic and Electron Velocity Fluctuations in Earth's Magnetosheath Downstream of a quasi-parallel bow shock

C.J. Pollock [a,*], J.L. Burch [b], A. Chasapis [c], B.L. Giles [d], D.A. Mackler [e], W.H. Matthaeus [c], C.T. Russell [f]

[a] Denali Scientific, 3771 Mariposa Lane, Fairbanks, AK, USA
[b] Southwest Research Institute, Division 15, PO Drawer 28510, San Antonio, TX 78228, USA
[c] Department of Physics and Astronomy, 217 Sharp Lab, University of Delaware, Newark, DE 19716, USA
[d] NASA Goddard Space Flight Center, 8800 Greenbelt Rd., Greenbelt, MD 20771, USA
[e] Catholic University of America, 620 Michigan Avenue NE, Washington, DC 20064, USA
[f] University of California, Los Angeles, 603 Charles Young Dr., Los Angeles, CA 90095-1567, USA

ARTICLE INFO

Keywords:
Turbulence
Magnetosheath
Intermittency

ABSTRACT

We present statistical single-spacecraft observations of magnetic and electron velocity fluctuations in Earth's magnetosheath, likely in the vicinity of the magnetopause, downstream of a bow shock immersed in quasi-parallel interplanetary magnetic field conditions, a situation conducive to plasma turbulence in the downstream flow. These fluctuations exhibit scale-dependent behavior, wherein histograms of their Partial Variance of Increments (PVIB or PVIVe) demonstrate highly non-Gaussian forms at small scales and are reasonably well-described by kappa distributions, albeit with fitted values of the kappa parameter only slightly larger than 1.5, exemplifying their power law nature at large values of PVI. At larger scales, the PVI histograms lose their non-Gaussian nature and are well described by both Gaussian and kappa distributions with large values of the kappa parameter. The PVI histograms furthermore exhibit kurtosis that increases with decreasing scale, a characteristic that is much more prominent in the magnetic fluctuations than in the electron velocity fluctuations. This feature that is not yet explained. In both cases, the results are characteristic of turbulent intermittency.

1. Introduction

Turbulence is common and very important in both nature and human applications such as fluid flow through pipes or blood vessels or around cars or aircraft elements. Wherever mass flows, turbulence will ensue under proper conditions and will thereby profoundly modify the flow. A fundamental characteristic of turbulent flow is that an observer is not able to predict the relevant state variables such as densities, velocities, and electro-magnetic fields in the case of plasma turbulence, given their initial values and the average force field along a trajectory. In the case of non-turbulent (laminar) flow, this capability exists. The state parameters of turbulent flow are therefore treated as random variables and statistical analysis is applied in attempts to gain insight into turbulent transport and dissipation processes. Kolmogorov (1941) first used a heuristic approach in attempting to describe turbulent energy transport across length scales in non-conducting fluids, from the largest macroscopic scales at which energy is injected into a turbulent system to the smallest molecular scales at which the energy is finally dissipated by viscosity. The range of scales between these two extremes was referred to as the inertial range. Here, Kolmogorov inferred a power law distribution of fluctuation energy with a $-5/3$ index. Such distributions have been commonly observed in the fluctuating velocity fields of non-conducting fluid turbulence, lending great credence to Kolmogorov's inference.

In collisionless plasma flow, no viscous effect is available to account for energy dissipation. Nevertheless dissipation in such plasmas is inferred to occur by some mechanism at small scales. This is based on the fact that power law distributions of energy content with $-5/3$ indices have been observed across a wide range of intermediate scales in

* Corresponding author.
E-mail addresses: craig@denaliscientific.org (C.J. Pollock), jburch@swri.edu (J.L. Burch), chasapis@udel.edu (A. Chasapis), barbara.giles@nasa.gov (B.L. Giles), david.a.mackler@nasa.gov (D.A. Mackler), whm@udel.edu (W.H. Matthaeus), ctrussell@igpp.ucla.edu (C.T. Russell).

https://doi.org/10.1016/j.jastp.2017.12.006
Received 30 June 2017; Received in revised form 19 October 2017; Accepted 7 December 2017
Available online 13 February 2018

turbulent solar wind magnetic fields (Bruno and Carbone, 2005), indicating energy transport from large to small scales. The question of how the energy is finally dissipated at small scales in collisionless plasma turbulence remains open. Another important characteristic observed in both fluid and, more recently, collisionless plasma turbulence is intermittency. That is, large fluctuations are seen to be embedded and spatially or temporally localized within the turbulent fields of both non-conducting and conducting fluids (Jimenez, 1998; Bruno and Carbone, 2005; Matthaeus et al., 2015), indicating that dissipation processes may be highly localized. In the case of collisionless plasma, large and localized fluctuations in the magnetic field components means that electric currents become concentrated within the turbulent flow, giving rise to the conjecture that magnetic reconnection at concentrated electric current sites in collisionless plasmas may be involved in the energy dissipation process.

Greco et al., (2008) introduced the Partial Variance of Increments (PVI) as a diagnostic for intermittent magnetic field fluctuations in turbulent plasma flows. The PVI, applied to magnetic field component fluctuations, referred to here as $PVIB_i$ is defined as:

$$PVIB_i(t,\ \tau) \equiv \frac{|B_i(t+\tau) - B_i(t)|}{\sqrt{\langle(\Delta B_i)^2\rangle}}, \tag{1}$$

where B_i is a fluctuating magnetic component, t is an observation time and τ is a time lag. The denominator in eq. (1) is the rms variability in the magnetic component over a time longer than τ. So, the $PVIB_i$ is a time history of B_i transition amplitudes (positive and negative), normalized by the B_i's longer term variability, at a cadence τ and with the clock starting at t. The $PVIB_i$ has been studied by numerous authors (Greco et al., 2008; Chasapis et al., 2015; Chasapis, 2015 and citations therein). It is not uncommon to apply Taylor's hypothesis (Taylor, 1938) of frozen in turbulence to interpret temporal observations at a point in terms of a fixed spatial field of turbulence flowing past the observer. Taylor (1938) submitted his hypothesis in the context of non-conducting fluid turbulence in the case where diffusive effects are small compared to convective effects, a turbulence-inducing situation referred to as high Reynolds number flow. Extensions of the Taylor Hypothesis to fields including MHD and collisionless kinetic plasma turbulence have proved to be interesting and fruitful avenues of investigation (see for example, Jokipii 1973)).

Although magnetic fluctuations have received the most attention in studying turbulence in space plasmas, other plasma variables can be expected to participate and display similar properties as magnetic field components. For Alfven-like fluctuations participation by plasma velocity may be expected, for example (Belcher and Davis, 1971). A PVI analysis may be applied not only to magnetic fields, but to the turbulent fluid velocity, electric field, or any neutral or conducting fluid state variable. Application to electron or ion plasma flows at relevant time cadences has not been possible in near-Earth space prior to the launch of NASA's Magnetospheric Multiscale (MMS) mission on March 13, 2015 (Burch et al., 2014), on which the Fast Plasma Investigation (Pollock et al., 2016) provides reliable electron and ion distribution functions and their moments at 30 ms and 150 ms cadence, respectively, when burst data rates are transmitted.

The PVI associated with a measured fluctuation time series should not be confused with the Probability Distribution Function (PDF) of fluctuation amplitudes associated with the time series. Simply put, the PVI is the normalized absolute value of the vector component increment, while the PDF is the normalized frequency of occurrence of values of the increments. The PDF is defined over a signed domain (positive and negative fluctuations), while the PVI is not. Only normalized size matters for PVI. The fluctuations in state parameters such as velocity and E&M fields in turbulent fluid (no E&M) and collisionless plasmas have shown themselves to be characterized by a large kurtosis in the PDF. That is, histograms of the signed turbulent magnetic fluctuations scaled by their long term variance, exhibit non-Gaussian behavior in the form of excesses in the large event amplitude tail of the distribution. This is most commonly diagnosed by measurement of the distribution's 4th moment, its kurtosis. Large kurtosis indicates a greater number of large amplitude events than would be expected from a Gaussian distribution, for which the normalized event amplitude falls off very steeply and large amplitude events are essentially non-existent. Non-Gaussian distributions are indicative of clumping into concentrations of both small and short time scale dynamics. This clumping concentrates energy and gradients that yield non-linear dynamics.

The question arises as to how one may identify a 'turbulent' plasma field in space plasma observations. Large magnetic Reynolds number is a natural criterion, but this is difficult to estimate in a collisionless plasma. Invoking a requirement for a Kolmogorov (1941) cascade, one might invoke a requirement on magnetic spectral power law dependency (search for −1.67) in some inertial range. One could look at the PDF of magnetic or other state variables or their time-lagged increments, with non-Gaussian high-kurtosis characteristics as good candidates or simply look for state variability that is of the same order or larger than the background variables. When working in a magnetosheath, one might filter on upstream IMF conditions, aiming to be downstream of a quasi-parallel bow shock, a condition that has been found to yield turbulence in the downstream magnetosheath. The answer to the question is not fully clear but some combination of these is undoubtedly required.

A question also arises as to how one should attempt to model the distributions of fluctuations observed in the state variables associated with a field of plasma turbulence. Gaussian statistics are clearly appropriate for uncorrelated fluctuations, just as they are in the cases of collision dominated plasma distributions in equilibrium, but what about turbulent field and plasma fluctuations on time and length scales at which significant higher order correlations exist? In space physics, it has been found repeatedly that 1D collisionless charged particle distribution functions exhibit good conformity to the kappa distribution (Pierrard and Lazar, 2010), given as:

$$f(v,\ \kappa) = \frac{n}{2\pi(\kappa W^2)^{3/2}} \frac{\Gamma(\kappa+1)}{\Gamma\left(\kappa - 1/2\right)\Gamma\left(3/2\right)} \left(1 + \frac{v^2}{\kappa W^2}\right)^{-(\kappa+1)}, \tag{2}$$

where Γ is the gamma function and, in the plasma distribution function context, n is the particle density, v is the particle speed, and W is the most probable speed. The kappa distribution has the properties that, at small values of κ, the particle distribution function has a prominent high energy tail, while at very large values of κ, the distribution function becomes identical to Gaussian. While no such interpretation as thermal speed or particle density is available in the context of non-Gaussian distributions of fluctuation in turbulent plasma, the functional form of the kappa distribution and its natural evolution from a form with a prominent power law-like tail at small κ to a more Gaussian form at large kappa makes it a convenient tool to characterize the distributions of fluctuation amplitudes in turbulent plasma.

In this paper, we examine an interval of turbulent plasma in Earth's magnetosheath, downstream of a quasi parallel bow shock and characterize observed fluctuations in the magnetic field and electron velocity components using the PVI introduced by Greco et al., (2008) and shown in Eq. (1), as functions the time lag (τ) between samples. We find that at small time lags there is a prominent tail in the large fluctuation end of the PVI distribution and that these distributions are reasonably well modeled by fitting to kappa distribution and not as well modeled with fitting to Gaussian distributions. At larger lags this characteristic disappears and the distributions are well-described by both Gaussian and kappa distributions, for which the fitted kappa index grows large. In Section 2, we provide a brief description of the MMS mission and the instrumentation used in the study. Section 3 includes presentation of the observations, the functional forms fitted to the derived fluctuation distributions and analysis of the fluctuation distributions 4th moment, or kurtosis, as a

function of the time lag applied to the analysis before concluding with a brief discussion of the results in Section 4.

2. Mission and instrumentation

Although numerous observations of kinetic plasma turbulence have been published over the years, very few have appeared in the literature from Earth's magnetosheath. Studies have typically focused on magnetic field observations, as observations of relevant plasma characteristics have had insufficient time resolution for such studies. NASA's Magnetospheric Multiscale (MMS) mission was launched on March 13, 2015 for the primary purpose of studying magnetic reconnection at sites within Earth's magnetosphere, notably on the day side magnetopause and in the night side geomagnetic tail (Burch et al., 2014). MMS consists of four identically instrumented spacecraft equipped with extensive plasma and field instrumentation and flying in a closely spaced tetrahedral formation for determination of 3D spatial gradients. The Fast Plasma Investigation (FPI) on MMS provides high quality 3D plasma distribution function measurements at burst-mode cadences (30 ms for electrons and 150 ms for ions) never before approached on space-borne plasma observatories (Pollock et al., 2016). The high cadence measurements are enabled by combining samples from eight top hat electrostatic analyzers (ESA's) for each species (ions & electrons) on each of the four spacecraft. The eight 180° fields of view extend from the spacecraft ± spin axes and are separated around the spacecraft belly band at 45°. Electrostatic FOV deflection by up to ±22.5° in azimuth angle allows filling in the 45° gaps between ESAs, enabling coverage of nearly 4π sr, limited only by the speed at which the high voltage power supplies can sweep and counting statistics at the short accumulation intervals. In this study, the fast plasma measurements are complemented by vector magnetic field measurements provided by the Flux Gate Magnetometer (FGM) experiment (Russell et al., 2016). Here, we present FGM Survey Mode magnetic measurements that provide the vector magnetic field components and magnitude at 62.5 ms cadence and Burst Mode FPI electron velocity component measurements at 30 ms cadence. While targeted for plasma and field dynamics expected to be observed within the small and fast-moving reconnection electron diffusion regions associated with reconnection sites, these high cadence plasma and field measurements are ideal for in situ study of turbulent plasma and field fluctuations and their correlations.

3. Observations

We present single-spacecraft plasma and magnetic field observations from MMS1 during a turbulent magnetosheath interval on January 24, 2016 (23:40:00–23:45:00). These observations were obtained during a period of quasi-parallel upstream solar wind conditions, the upstream solar wind ram pressure was moderate at 1.7 ± 0.4 nPa, and the IMF Bz was near +2 nT. During the event, 5 min of contiguous burst data were recorded inside the magnetosheath, providing a rare opportunity to look at the PDFs and PVI of not only the magnetic fluctuations that are always available at 0.0625 ms cadence in the MMS fast survey data, but also the plasma electron velocity fluctuations, available during burst mode at 30 ms cadence.

Fig. 1 shows an overview of the interval in question. In Fig. 1a (top), we present the three components of the fluctuation magnetic field in the top panel and energy-time spectrograms of ions (Figure 1a, 2nd panel) and electrons (Figure 1a, 3rd panel) during a 1-h interval from 2 300 UT to 2 400 UT that includes the 5-min burst period of interest. The magnetic field exhibits strong variations in all three components and the ion flux shows quasi-periodic variations throughout the interval. The electron flux signature appears substantially more smooth than that of the ion flux. The plasma density (not presented) shows irregular variations between 20 cm^{-3} and 70 cm^{-3} through the interval. A 5-min segment of magnetic survey data is shown in Fig. 1b (top panel) and plasma burst resolution data is shown in the 2nd, 3rd and 4th panels of Fig. 1b. Ion flux is again shown in Fig. 1b (2nd panel) in spectrogram format, followed by ion (3rd panel) and electron (fourth panel) bulk velocities. A couple of the quasi-periodic ion flux drop-outs that are not well resolved in Fig. 1-a (2nd panel) are well resolved in the 2nd panel of Fig. 1b. It can be seen that at the times of the flux dropouts, the x-components of the ion and electron bulk velocities become large and negative indicating fast anti-sunward flow. It would be tempting to attribute this to entry into the solar wind. However, the moderate solar wind ram pressure, the absence of any apparent solar wind flux signature in the ion spectrogram, and the retention of relatively high plasma densities argue against such an interpretation. Fig. 1c shows the orbit of the MMS spacecraft at the time of these observations. It can be seen there that MMS was located in in the morning side magnetosheath, downstream from a solar wind impact point on the bow shock at later magnetic local times. The IMF at the location of ACE during a 30-min interval an hour before the magnetosheath observations was measured to be (4.6, −2.0, 0.91) nT, yielding an orientation in the ecliptic as illustrated in Fig. 1c, and extending 26° out of the plane of the diagram toward the viewer.

Fig. 2 shows time series of the increments for the measured magnetic field (Fig. 2a) and electron velocity (Fig. 2b) GSE vector components x, y and z, in the case of a single-sample lag (30 ms for electron velocity and 62.5 ms for magnetic field). The plotted values are signed quantities. The PVIs defined in Eq. (1) are derived as the absolute values of the normalized x-component data in Fig. 2, in the cases of single-sample lag. In each panel, the x-component is offset 15 units in the positive direction and the z-component is offset 15 units in the negative direction for clarity of presentation. The time lag (τ) is the natural acquisition cadence of the measurements: 62.5 ms in the case of the Fast Survey magnetic measurements and 30 ms in the case of the Burst electron velocity measurements. A high degree of variability is seen in all of these time series, with large amplitude intermittent fluctuations in evidence. The large fluctuations in the magnetic components are correlated with one another, as are those associated of the electron different velocity components. However, the magnetic and electron velocity components are not expected to be closely temporally correlated with one another as they would be, for example, if we were studying fluctuations in electron pressure, owing to the requirement for pressure balance. The intermittency evident in the fluctuation time series presented in Fig. 2 is characteristic of turbulent fluctuations.

In Fig. 3 normalized PVI histograms (number of events normalized to the maximum in the histogram) are plotted versus the PVI value as defined in Eq. (1). In the top panel, we examine the distribution of PVIBx, which is the PVI associated with the GSE x-component of magnetic fluctuations during the 5-min interval, at the FGM Survey single sample lag of 62.5 ms. In the bottom panel, it is the distribution of PVIVx, the GSE x-component of electron bulk velocity fluctuations during the same 5-min interval, at the FPI Burst single sample lag of 30 ms. Error bars shown are based on Poisson statistics of the non-normalized histogram. We show the histogram data as scatter plots with dashed and solid curves showing normalized Gaussian distribution (single parameter) and normalized kappa distribution (two parameter) fits, respectively. The normalized distributions are used for the sake of simplicity, as we are only trying to capture the shape of the distributions. Fitting is performed using mpfit. pro, which implements nonlinear least squares fitting in IDL based on the Levinburg-Markuardt algorithm and returns one-sigma uncertainties in the fitted parameters based on provided one-sigma uncertainties in the data, as represented by the error bars shown in the figure. The fitted functions are defined as:

Gaussian distribution:

$$f(x) = e^{\frac{-x^2}{\kappa_0}} \tag{3a}$$

Kappa distribution:

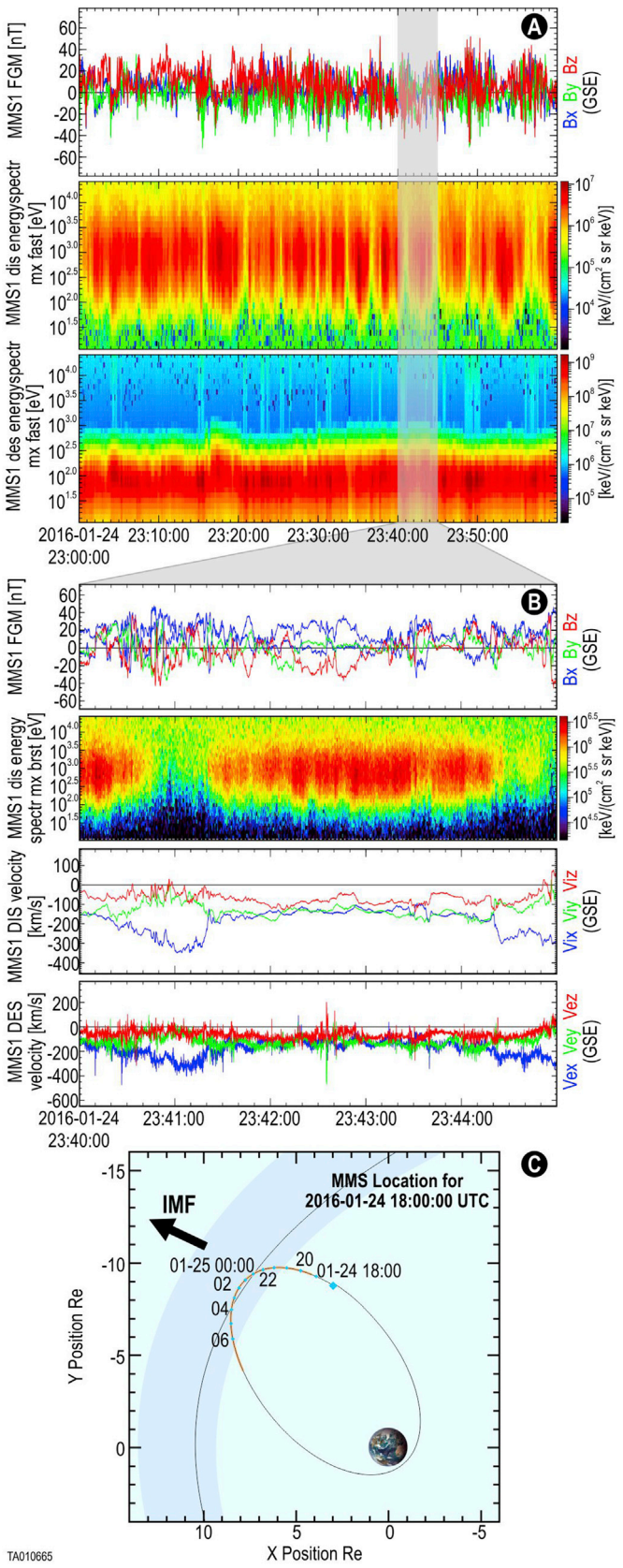

(caption on next column)

Fig. 1. A) GSE components of the magnetic field (top) and ion and electron energy-time spectrograms (2nd and 3rd panels) are plotted versus UT; B) a 5-min interval of magnetic and plasma observations from MMS is plotted versus UT. The top panel contains vector magnetic field measurements from the flux-gate magnetometer at the FGM survey cadence of 62.5 ms. The colors denote magnetic vector components in the standard MMS sequence of x: blue, y: green and z: red. The 2nd panel contains differential directional ion energy flux color coded on the logarithmic scale to its right and plotted versus ion energy/charge, whose scale appears to the left of the panel. The bottom two panels display ion (2nd from bottom) and electron (bottom) bulk velocities. The bulk velocity components are color coded in the same manner as the magnetic field components. All the ion data is presented at 150 ms cadence. The electron data is presented at 30 ms cadence; C) The orbit of the MMS spacecraft is shown in the GSE x-y plane, beginning at 1800 on January 24, 2016. The shaded region indicates the 1-sigma model location of the magnetopause, with the most probable location shown as a thin line. The orientation of the IMF projected onto the plane is indicated. It makes a 17° angle in the plane with the GSE-X axis and extends 23° out of the page. (For interpretation of the references to color in this figure legend, the reader is referred to the Web version of this article.)

$$f(x) = \left(1 + \frac{x^2}{\kappa W^2}\right)^{-(\kappa+1)} \tag{3b}$$

The single fitted parameter in the Gaussian case is x_0. In the kappa case, the two fitted parameters κ and a parameter subsumed in W^2 to be defined below. In the common application of the kinetic single particle distribution function modeled either as a Gaussian or kappa distribution, x is interpreted as the independent variable particle speed or velocity component, and x_0, or W in the kappa distribution case, is interpreted as a most probable speed or thermal speed. Here, W is defined as (Pierrard and Lazar, 2010):

$$W^2 \equiv (2\kappa - 3)\frac{x_{0\kappa}^2}{\kappa}, \tag{4}$$

where $x_{o\kappa}$ is the second of the two kappa distribution fit parameters. In the application of these formulas to PVI histograms of magnetic and electron bulk velocity component fluctuations, the interpretations of W and x_0 are not defined. We use them here simply as empirical diagnostics in a statistical observation of these state variables. The kappa distribution is defined for all real values of κ greater than 1.5, below which the function becomes undefined. At small values of kappa, approaching 1.5 from above, the power law characteristic at larger values of x becomes more pronounced, while large values of κ yield a more Gaussian characteristic. The fitted values of κ in Fig. 3, slightly larger than 1.5, demonstrate the prominence of the power law tail in these distributions. Each panel in Fig. 3 shows a tabulation of the fitted parameters and their one-sigma uncertainties. In the case of the kappa distributions, fitted values of the κ parameter are constrained in the fitting routine to remain larger than 1.5. We also note that the uncertainties in the values of $x_{o\kappa}$ are much larger than the values themselves, a matter for future study. We characterize the goodness of the fits by computing and tabulating values of the reduced chi-squared for both the Gaussian and kappa fits in Fig. 3. We limit that characterization to the region of interest, that is the large PVI tails, by limiting the range of PVI values over which the reduced chi-squared parameters are computed to ≥1.0 and limiting the degrees of freedom appropriately.

The distributions in Fig. 3 demonstrate non-Gaussian statistics in both the magnetic and electron velocity components with the large event tail of the distributions being their outstanding features. The single-parameter Gaussian fits can not capture the large PVI tail (RCSG = 12.9 and 8.4 for Gaussian fits to Bx and Vex, respectively) and even the kappa distribution is unsuccessful in capturing it in the magnetic component fluctuations (RCSK = 4.7), though it does an excellent job with the electron velocity component fluctuations (FCSK = 0.7). In both cases the Gaussian model falls off abruptly compared with either the data or the kappa fit.

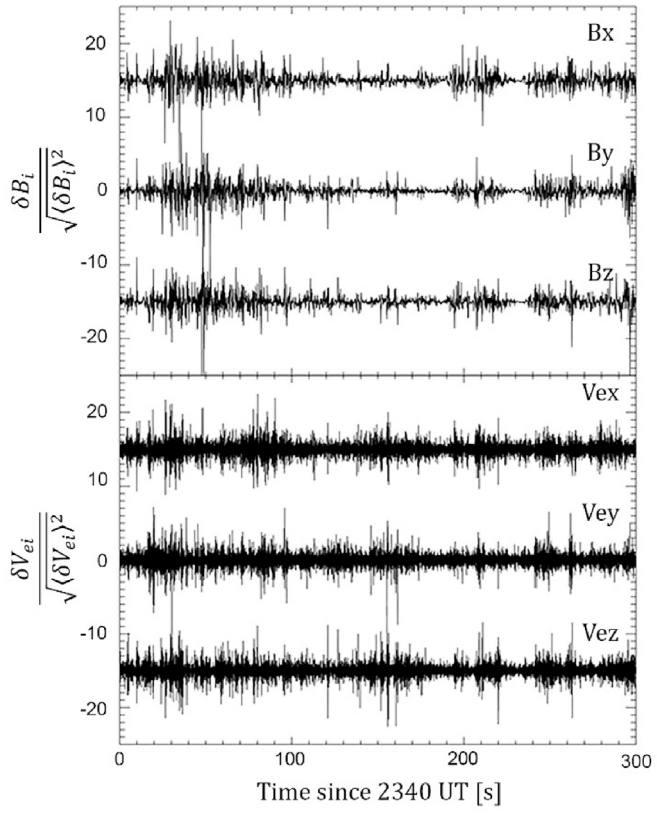

Fig. 2. Time series of GSE (x, y, z) components of A) magnetic and B) electron bulk velocity normalized vector component fluctuations versus time, in seconds, for a 5-min (300 s) interval from 2 340 UT to 2 345 UT on January 24, 2016.

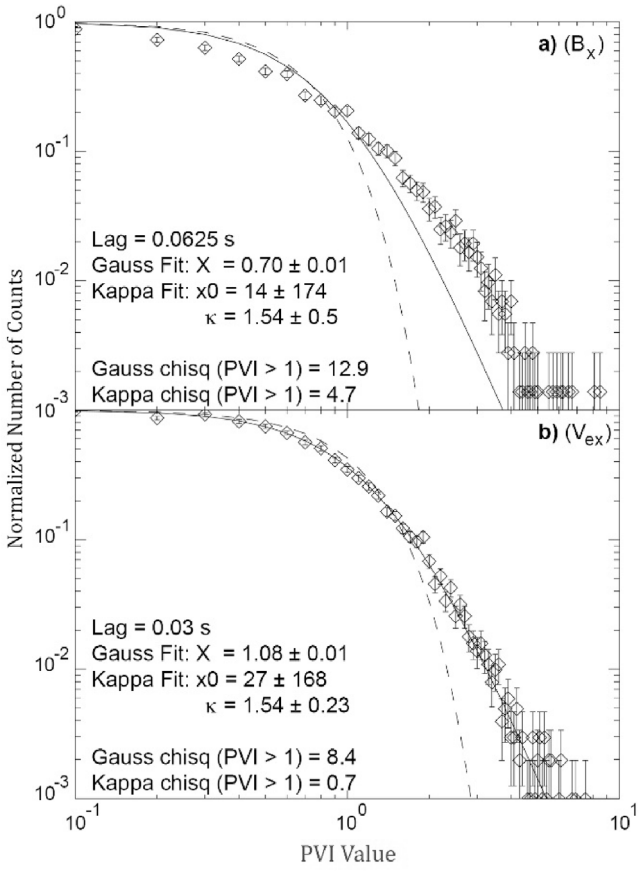

Fig. 3. Normalized histograms of the Partial Variance of Increments (PVI) for fluctuations for the 5-min shown in Fig. 2, in a) the magnetic field GSEx-component with τ = 62.5 ms and b) the electron bulk velocity GSEx-component with τ = 30 ms. The error bars are based on Poisson statistics applied to the non-normalized histograms. Two fits to the data are shown, one (dashed curves) is a normalized Gaussian fit and the other (solid curves) is a normalized kappa distribution model. Fit parameters, their error estimates, and reduced chi-squared parameter for both models are listed. Note that the reduced chi-squared parameter was only computed over the PVI range ≥1.0, in order to quantify goodness of fit in the tail region of the distribution. See details in text.

In contrast with the single-sample lag used in the data of Figs. 3 and 4 (same format as Fig. 3) shows histograms of PVI values computed using a time lag of approximately 2 s (32 samples in the case of the FGM B_x component and 64 samples for the FPI V_{ex} component). In this case, the large event tails in the histograms, while still evident, are not as pronounced as in the shorter lag case of Fig. 3. The Gaussian fits are still unable to capture the large event tails, with RCSG = 8.8 and 6.4 for the magnetic and velocity fluctuations respectively. The kappa distribution fits capture them much better: RCSK = 2.0 and 1.4 for the magnetic and velocity fluctuations. Fitted values of κ are still seen to be only slightly larger than 1.5, indicating the continued prominence of the power law behavior in the large event tail.

Fig. 5, in the same format as Figs. 3 and 4, shows normalized PVI histograms of Bx and Vex at even larger lags of approximately 30s (512 samples for the FGM data and 1 024 samples for the FPI Vex data). In these cases, the histograms have become well-described by the Gaussian model, the power law behavior in the large event tails of the distributions has essentially disappeared, both the Gaussian and kappa distribution fits do a fairly good job of representing the data and the two fitting models have nearly coalesced, becoming difficult to distinguish from one another. The fitted values of κ have now grown away from the singular value of 1.5, approaching a value of 4 in the case of the magnetic fluctuations and equal to 9 in the case of the electron velocity fluctuations. Thus we observe a progression from the small lag case of Fig. 3 where the PVI histograms are far from Gaussian and feature prominent power law tails and fitted values of κ only slightly larger than 1.5, to the large lag case of Fig. 5 where the PVI histograms become Gaussian, the power law tails have disappeared, and the kappa distribution fits exhibit larger values of kappa, indicating coalescence of the Gaussian and kappa distribution models. This progression represents a scale dependent behavior of the statistics of the magnetic and electron velocity component fluctuations under study.

Another demonstration of this progression is presented in Fig. 6, where we plot the excess kurtosis of the signed fluctuation PDF (of which the PVI is the absolute value) for the magnetic and electron velocity component fluctuations versus the sampling time lag during our 5-min study interval. In this case, the excess kurtosis was measured for each of the three vector magnetic and electron velocity components were averaged together and plotted. The error bars shown represent the standard deviation among the three quantities comprising the average and are seen to be quite large, particularly in the case of the magnetic fluctuations at lags smaller than 1 s. The excess kurtosis is defined as the kurtosis minus 3.0. The kurtosis is the fourth moment of the PDF normalized by the square of the second moment (i.e., the square of the variance). It measures the prominence of events in the tail of the PDF and is equal to 3.0 for a Gaussian distribution, is larger for PDFs with prominent tails and smaller for distributions that fall off faster than a Gaussian distribution would. Thus the excess kurtosis plotted in Fig. 6 is characterized by large values at small time lags and falls to near zero at larger time lags, indicative of distributions with prominent large event tails at small lags and progressing to much more Gaussian behavior at the larger lags. The distinct difference at time lags less than 1 s in the excess kurtosis for the magnetic fluctuations, which continues to increase at smaller values of lag, compared to that for the electron velocity component fluctuations, which flattens out at lags less than 1 s to a value near 7

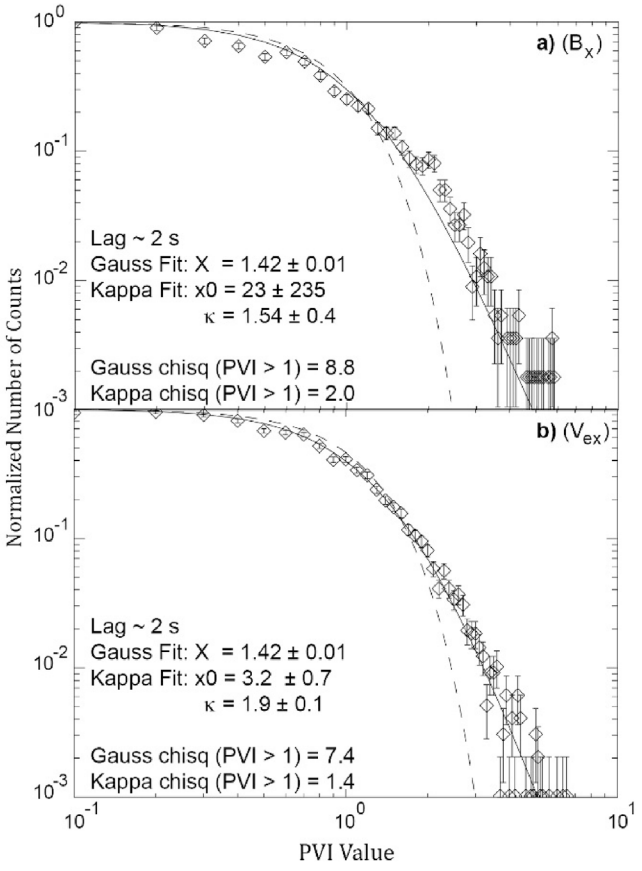

Fig. 4. Same as Fig. 3, with a 2 s lag.

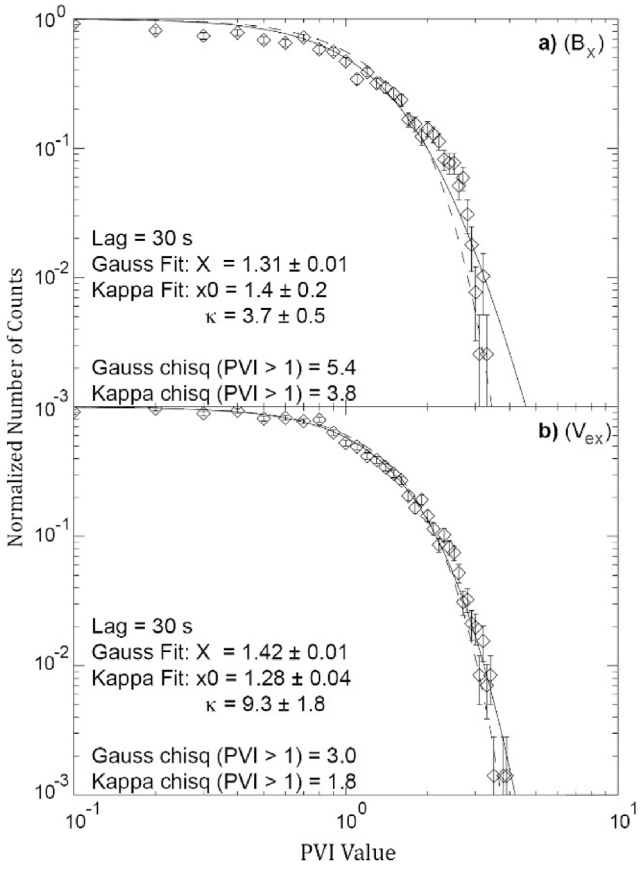

Fig. 5. Same as Fig. 3 with a ~32 s lag.

or 8 is remarkable, though the uncertainty represented by the large error bars in that region is substantial. Whether this is a persistent feature in turbulent plasma fluctuations such as these will be the subject of a future study.

4. Discussion

We have presented single spacecraft MMS1 observations from Earth's magnetosheath during an interval when the IMF orientation with respect to Earth's magnetospheric bow shock is in a quasi-parallel configuration. Such an interval is expected to produce turbulent plasma conditions in the downstream magnetosheath. We have examined magnetic and electron bulk velocity fluctuations during this interval and found that these fluctuations exhibit characteristics associated with kinetic plasma turbulence, namely intermittency. This is diagnosed by 1) inspection of the fluctuation time series in Fig. 2 and 2) non-Gaussian distributions in the fluctuation PDFs at small lags, measured as excess kurtosis as demonstrated in Fig. 6, and kappa vs Gaussian fits to PVI histograms at small lags, exemplified in Figs. 3 and 4. At larger lags, non-Gaussian nature of the fluctuations is not observed, as seen in both Figs. 5 and 6. Perhaps surprisingly, Fig. 2 illustrates that the fluctuation time series at highest time resolution (shortest lags) are not strongly temporally correlated between the magnetic and electron velocity components. However, the individual components in the field fluctuations are much better correlated with each other, as are the components of the electron velocity fluctuations.

The context for these measurements has been provided in Fig. 1. The background plasma conditions show a large scale (Fig. 1A and B) variability with characteristic time scale of a few minutes. Periodically the magnetosheath ion flux drops out with a more tenuous and hotter component remaining. At these times the GSE-x component of the plasma ion velocity becomes large and negative (Earthward). It must be that

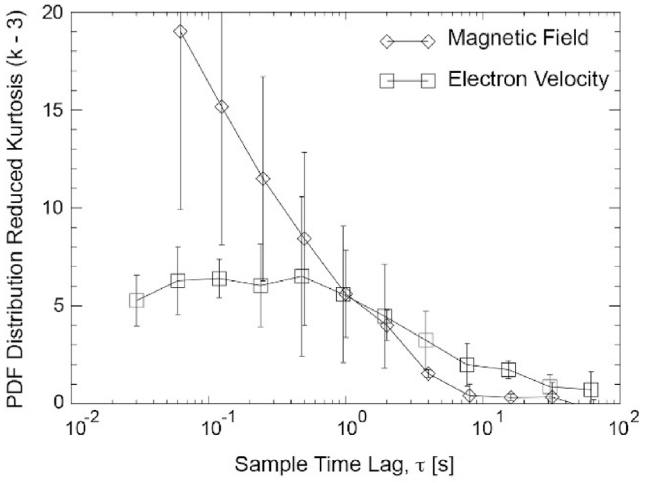

Fig. 6. Excess kurtosis (kurtosis-3) of the fluctuation probability distribution (PDF) of magnetic and electron velocity component fluctuations, plotted vs the increment time lag. Error bars are derived as the standard deviation among the excess kurtosis measured among the three vector components in each case. See text for further description.

MMS is located very near the magnetopause, which is either moving in and out or contains a surface wave that brings troughs and crests propagating past the spacecraft. The 5-min interval analyzed in this study contains plasma and fields through a complete cycle of this kind and therefore, undoubtedly, represents a mixture of plasma and field signatures from the populations cyclically sampled as described above. It will be interesting to segregate these populations and look more closely at them individually.

An interesting question arises as to the meaning of the statistical results obtained here and in other studies of intermittency. It is well known that turbulent fluids (neutral or plasma) display intermittent behavior like that illustrated here. The large kurtosis in magnetic PDFs acquired at short temporal (or spatial, applying the Taylor hypothesis) lags and disappearing at longer lags has been demonstrated (Chasapis et al., 2015; Burlaga and Viñas, 2005) in the past. This behavior is reminiscent of the Poisson interval distribution that characterizes, for example the intervals between arrivals of raindrops on a surface, those occurring between emissions from a radioactive substance, or those between events recorded on a particle detector near the exit of an electrostatic analyzer. At some average event rate, in all these cases, the most probable intervals between events are in fact favored on the short interval end and are shorter than the average interval. The analogy is not exact and the intermittent structures immersed in the plasma under study in this event likely do not conform to the Poisson interval distribution. However, the question as to the statistics governing interval distributions associated with intermittent structures in a turbulent field is brought to mind.

We have noted the much more dramatic increase in the kurtosis at small scales associated with the magnetic fluctuations as compared with the electron velocity fluctuations, an intriguing result. We have also noted, however, the large error bars associated with the magnetic kurtosis measurement. These error are computed as the standard deviation among three measurements at each lag (e.g., PVI associated with Bx, By, Bz). Further analysis is required to determine the persistence of this result and its origin. In all cases, we have thus far considered the time domain lag used in computing PVI histograms at various scales. As we alluded in our introduction, it is common in both fluid turbulence studies and, more recently, those focused on plasma phenomena to invoke Taylor's hypothesis (Taylor, 1938) to interpret such lags in the spatial domain, invoking the notion of a fixed system of spatial oscillations convecting in the background flow, past the observation point. In this case, spatial lag is proportional to the time lag with a constant of proportionality equal to the value of the background flow speed which, for the 5-min interval under study is (246 ± 42) km/s, based on the FPI ion flow measurements and their standard deviation. Therefore, the spatial lags associated with the fitted histograms in Figs. 3–5 are then 7/3 km for the magnetic/velocity fluctuations of Figs. 3 and 500 km for Figs. 4 and 7 500 km for Fig. 5. Similarly, the spatial domain of Fig. 6 extends from 7 km to greater than 25,000 km. There is a clear flattening of the magnetic kurtosis curve near 10 s (2 500) km and some indication of spectral breaks for both the magnetic and electron velocity kurtosis near 1 s (250 km). For comparison, we note that the local ion gyroradius and inertial length near 90 km and 40 km, respectively.

The relevance of studies of plasma turbulence to MMS, whose sole prime mission is to study both the fundamental physics of magnetic reconnection and its impacts on our local space environment lies in likely connections between the two phenomena. Magnetic reconnection produces high speed outflows that are subject, therefore, to turbulence. As to the potential importance of turbulence to reconnection, there are at least two areas where relevant questions reside. First, how is reconnection modified when the background plasma is turbulent, compared with when it is not? Second, are the concentrated electric currents that give rise to the concentrated magnetic field variations the sites of energy dissipation and perhaps a significant sink at the small scale end of a Kolmogorov-type energy cascade through scales? For more general discussion of these issues, see Matthaeus & Velli (2011).

Though MMS is nearly ideally suited to the study of plasma turbulence in Earth's magnetosheath, the burst mode data is only rarely transmitted during periods in the magnetosheath, far from boundaries. The burst mode data is, after all, rightfully focused on boundaries, particularly the magnetopause in Phase-1, where magnetic reconnection is most prominently operating. Beyond that, MMS electric and magnetic field observations are always available at time resolutions fully sufficient for more detailed and multi-point studies of magnetosheath and solar wind turbulence. Combined with the plasma observations currently available from MMS and those to be obtained in the extended mission, which will undoubtedly contain ample burst data from deep within both the magnetosheath and the solar wind, much progress will be made in understanding collisionless plasma turbulence and its connections to magnetic reconnection in the future.

5. Conclusions

We have studied a short interval, January 24, 2016 at 2 340–2 345 UT, of plasma and magnetic field data acquired by MMS1 near Earth's pre-noon magnetopause during a period of quasi-parallel upstream IMF conditions. The interval was characterized by large scale (several minute) background variations in the character of the ion flux and background ion velocity during which apparently turbulent intermittent fluctuations in both the magnetic field and electron bulk velocity were observed. These fluctuations clearly demonstrate similar systematic behavior as functions of time scale or, in the case where the Taylor hypothesis is valid, spatial scale. At short scales of less than a few seconds, the PVI distributions of both magnetic and electron fluctuations demonstrated highly non-Gaussian behavior reasonably well characterized by kappa distributions with values of kappa approaching 1.5, a singular extreme in the domain for which the kappa distribution is defined and near which the power law nature of the PVI distribution becomes dominant. At larger scales, near 30 s in this case, the magnetic and electron velocity PVI histograms both transition to Gaussian, well fit by both equivalent Gaussian and large-κ valued kappa distributions and exhibiting negligible excess kurtosis. The evolution of PVI kurtosis with scale is dramatically different in the magnetic and electron velocity cases at small scales, though this result can only be considered preliminary and will be further investigated in future work. Features of intermittent turbulence, familiar in ordinary neutral fluids at high Reynolds numbers (Antonia et al., 1984), have been observed in the solar wind (Sorriso-Valvo et al., 1999; Kiyani et al., 2009) and in the magnetotail (Osman et al., 2015). They are here demonstrated in Earth's magnetosheath in both magnetic and electron velocity fluctuations using state of he art instrumentation aboard the MMS mission.

Acknowledgements

This research was supported by the National Aeronautics and Space Administration (NASA) Magnetospheric Multiscale Mission (MMS) in association with NASA contract NNG04EB99C. Institut de Recherche en Astrophysique et Planétologie (IRAP) contributions to MMS FPI were supported by Centre National d'Études Spatiales (CNES) and Centre National de la Recherche Scientifique (CNRS). We thank the entire MMS team and instrument leads for data access and support. The data presented in this paper are the L2 data of MMS and can be accessed from MMS Science Data Center (https://lasp.colorado.edu/mms/sdc/public/). Funding for work at Denali Scientific was provided by GSFC Task 673.0-008, through the ADNET Corporation.

References

Antonia, R.A., et al., 1984. Temperature structure functions in turbulent shear flows. Phys. Rev. https://doi.org/10.1103/PhysRevA.30.2704.
Belcher, J.W., Davis Jr., L., 1971. J. Geophys. Res. 76, 3534.
Burch, J.L., et al., 2014. Magnetospheric Multiscale overview and science objectives. Space Sci. Rev. https://doi.org/10.1007/s11214-015-0153-z.
Burlaga, L.F., Viñas, A.F., 2005. Tsallis distributions of the large-scale magnetic field strength fluctuations in the solar wind from 7 to 87 AU. J. Geophys. Res. 110, A07110 https://doi.org/10.1029/2005JA011132.
Bruno, R., Carbone, V., 2005. Living Rev. Sol. Phys. 2, 4. https://doi.org/10.12942/lrsp-2005-4.
Chasapis, A., 2015. Study of Magnetic Reconnection in Turbulent Plasma Using Satellite Data. Astrophysics [astro-ph]. Universit´e Paris Sud - Paris XI.
Chasapis, A., et al., 2015. Thin current sheets and associated electron heating in turbulent space plasma. ApJL 804 (L1).
Greco, A., Chuychai, P., Matthaeus, W.H., Servidio, S., Dmitruk, P., 2008. Intermittent MHD structures and classical discontinuities. Geophys. Res. Lett. 35, L19111 https://doi.org/10.1029/2008GL035454.

Jimenez, J., 1998. Intermittency in small scale turbulence. Eur. J. Mech., B/Fluids 17 (n0), 405–419.
Jokipii, J.R., 1973. Annu. Rev. Astron. Astrophys. 11, 1.
Kiyani, K.H., et al., 2009. Global scale-invariant dissipation in collisionless plasma turbulence. Phys. Rev. Lett. 103, 7. https://doi.org/10.1103/PhysRevLett.103.075006.
Kolmogorov, A.N., 1941. C.R. Acad. Sci., U.S.S.R 30 (301), 538.
Matthaeus, W.H., Velli, M., 2011. Space Sci. Rev. 160, 145. https://doi.org/10.1007/s11214-011-9793-9.
Matthaeus, W.H., et al., 2015. Intermittency, nonlinear dynamics and dissipation in the solar wind and astrophysical plasmas. Philosophical transactions Series A, Mathematical, physical, and engineering sciences 373 (2041), 20140154. https://doi.org/10.1098/rsta.2014.0154.
Osman, K.T., et al., 2015. Multi-spacecraft measurement of turbulence within a magnetic reconnection jet. Ap. J. Lett. 815, 2.
Pierrard, V., Lazar, M., 2010. Kappa distributions: theory and applications in space plasmas. Sol. Phys. 287 (N° 1), 153–174. https://doi.org/10.1007/s11207-010-9640-2.
Pollock, C., et al., 2016. Fast plasma investigation for magnetospheric Multiscale. Space Sci. Rev. 199 (1–4), 331–406. https://doi.org/10.1007/s11214-016-0245-4.
Russell, C., et al., 2016. The magnetospheric Multiscale magnetometers. Space Sci. Rev. 199 (1–4), 189–256. https://doi.org/10.1007/s11214-014-0057-3.
Sorriso-Valvo, L., et al., 1999. Intermittency in the solar wind turbulence through probability distribution functions of fluctuations. Geophys. Res. Lett. 26, 13. https://doi.org/10.1029/1999GL900270.
Taylor, G.I., 1938. The spectrum of turbulence. Proc. Roy. Soc. Lond. A 164, 476.